Available online at www.sciencedirect.com
ScienceDirect
Journal of Power Sources 172 (2007) 388–394
JOURNAL OF POWER SOURCES
www.elsevier.com/locate/jpowsour

$NiSb_2$ as negative electrode for Li-ion batteries: An original conversion reaction

C. Villevieille, C.-M. Ionica-Bousquet, B. Ducourant, J.-C. Jumas, L. Monconduit *

Institut Charles Gerhardt, Laboratoire des Agrégats, Interfaces et Matériaux pour l'Energie, Université Montpellier II, Place E. Bataillon, Bat. 15, cc15, 34095 Montpellier Cedex 5, France

Received 14 March 2007; received in revised form 25 May 2007; accepted 24 June 2007
Available online 5 July 2007

Abstract

The study of the electrochemical reaction mechanism of lithium with $NiSb_2$ intermetallic material is reported here. The nickel diantimonide prepared by classic ceramic route is proposed as possible candidate for anodic applications in Li-ion batteries. The electrochemical characterisation of $NiSb_2$ versus Li^+/Li^0 shows a reversible uptake of 5 lithium per formula unit, which leads to reversible capacities of 500 mAh g^{-1} at an average potential of 0.9 V. From *ex situ* XRD and ^{121}Sb Mössbauer measurements it was shown that during the first discharge the orthorhombic $NiSb_2$ phase undergoes a pure conversion process ($NiSb_2 + 6\,Li^+ + 6e^- \rightarrow Ni^0 + 2Li_3Sb$). During the charge process that follows, the lithium extraction from the composite electrode takes place through an original conversion process, leading to the formation of the high pressure $NiSb_2$ polymorph. This highly reversible mechanism makes it possible to sustain 100% of the specific capacity after 15 cycles.

Keywords: Conversion reaction; Negative electrode; Lithium ion batteries; Nickel diantimonide; Electrochemical process; Capacity retention

1. Introduction

Exploration of new negative electrode material with high energy density and long lifetime is required for the development of the next generation lithium-ion batteries. Over the past few years, some Sb-based intermetallic compounds, such as $CoSb_3$ [1–4], $FeSb_2$ [5] and $CrSb_2$ [6], have been intensively investigated as negative electrodes for lithium ion batteries. These materials have shown higher capacities than the commercialized carbon material but suffer from poor cycle life. Attempts of cycle life improvements were realised using intermetallic compounds that undergo a phase transition to a lithiated intermediate compound with related structures, i.e. Cu_2Sb and $LiCu_2Sb$ [7], but the capacity retention was not improved. More recently, searching for the benefits of nanomaterials it was shown that simple compounds can electrochemically react towards Li through conversion reactions leading to sustainable reversible high capacities. As compared to the classical insertion reactions, which are limited to $1e^-$ even $0.5e^-$ transfer per 3d metal atom ($LiCoO_2$), these new conversion reactions can involve up to 3*y*Li per transition metal and enable a capacity gain of the battery. These reactions (Eq. (1)) proceed through a transformation of MX_y raw material into a composite electrode made up of metallic nanosized particles embedded in a Li_3X matrix:

$$MX_y + 3yLi \rightarrow yLi_3X + M^0\,(X = P,\ As,\ Sb) \qquad (1)$$

The pristine compound is restructured on charge. This type of reaction was initially demonstrated for oxides [8], and more recently asserted for phosphides [9]. In the case of the NiP_2–Li electrochemical system, we showed that the cubic and monoclinic NiP_2 phases react towards Li through a conversion or an insertion/conversion process, respectively, which makes for a good cycling stability, i.e. 900 mAh g^{-1} after 20 cycles. In the antimonide family, MnSb was also described as showing a conversion reaction towards Li with a reconstruction of the starting material at the end of the charge process [10]. Due to this reversible conversion, a 360 mAh g^{-1} capacity can be maintained after 15 cycles for the MnSb-based cells.

Owing to the positive aspect of the conversion reaction, especially in the case of NiP_2 and MnSb systems, we focus on the electrochemical study of the binary $NiSb_2$ phase. The electro-

* Corresponding author. Tel: +33 4 67 14 33 35; fax: +33 4 67 14 33 04.
E-mail address: laure.monconduit@univ-montp2.fr (L. Monconduit).

0378-7753/$ – see front matter © 2007 Elsevier B.V. All rights reserved.
doi:10.1016/j.jpowsour.2007.06.256

chemical behavior of nanosized $NiSb_2$ versus Li was recently reported by Xie et al. [11]. In this article, the nanosized intermetallic compound $NiSb_2$ was prepared by a solvothermal route. The authors studied the powder morphology effect on the electrochemical performance through a comparison between the micrometer sized $NiSb_2$, prepared by a levitation-melting/ball-milling route, and the $NiSb_2$ obtained by solvothermal route. In both cases, a poor capacity retention was obtained. The electrochemical mechanism was not discussed by the authors.

Regarding the high theoretical specific capacity (greater than 500 mAh g^{-1}) of $NiSb_2$ we decided to explore this new potential negative electrode material. The paper is organized as follows: firstly the experimental part describes the synthesis and chemical/physical characterisations of $NiSb_2$ and secondly the electrochemical analysis and performance, *ex situ* X-ray and ^{121}Sb Mössbauer measurements are presented together with the attempts to determine the electrochemical mechanism.

2. Experimental

2.1. XRD and SEM

X-ray diffraction (XRD) measurements on powdered $NiSb_2$ samples were performed on a Philips X-pert diffractometer using the Cu Kα radiation. For the *ex situ* XRD measurements, the *C*/3 (1 Li/3 h) rate cycled cells were dismantled in an Ar filled glove box and the electrodes were covered with PE (polyethylene) film in order to avoid air exposure. The powder morphology of pristine materials was determined by scanning electron microscopy (SEM).

2.2. Electrochemical tests

Swagelok-type cells were assembled in an argon filled glove box and cycled using a Mac Pile automatic cycling/data recording systems (Biologic Co., Claix, France) in a potential window between 2.5 V (or 2 V) and 0.02 V versus Li^+/Li^0 and a cycling rate of *C*/*n* (that is one lithium per formula unit in *n* hours). These cells comprise a Li metal disc as the negative electrode, a Whatman GF/D borosilicate glass fiber sheet saturated with a 1 M $LiPF_6$ in ethylene carbonate (EC), dimethyl carbonate (DMC) (1:1 in w/w) as the electrolyte, a positive electrode made after mixing the starting nickel antimonide powder with 15 wt% carbon black (SP). Usually, 10–12 mg of the mixed powders was placed on top of the Swagelok plunger.

2.3. Mössbauer

^{121}Sb Mössbauer measurements were performed using a ^{121m}Sn in $BaSnO_3$ source of nominal activity 0.4 mCi on an EG and G constant acceleration spectrometer in transmission mode. During the measurements, both source and absorbers were simultaneously cooled down to 4 K in order to increase the fraction of recoil-free absorption and emission processes. The zero isomer shift was defined from the spectrum of InSb at 4 K ($\delta = -8.72(4)$ mm s^{-1} relative to the $Ba^{121m}SnO_3$). Measurements were performed *ex situ* at several depths of discharge and charge. The Swagelok cells were stopped and opened inside a dry box once cycled down to the required voltage. The partially lithiated material was recovered and placed on specific sample holders transparent to the γ-rays.

3. Results

3.1. Synthesis and characterisation

The orthorhombic $NiSb_2$ phase was synthesized at high temperature by placing stoichiometric amounts of nickel metal (Ni Alfa Aesar, 350 mesh, 99.9%) and antimony (Sb Alfa Aesar, 350 mesh, 99%) powders in a sealed evacuated silica tube. The tube was placed into a furnace, and the temperature was increased to 600 °C using a ramp of 5 °C min^{-1}, and held to this temperature for 4 days. The samples were air-quenched. The XRD pattern of $NiSb_2$ is depicted in Fig. 1 and reveals sharp Bragg peaks, indicative of a highly crystalline sample, which could all be indexed on the basis of an orthorhombic marcasite $NiSb_2$ cell with the following refined lattice parameters: $a = 5.180(2)$ Å, $b = 6.312(2)$ Å, $c = 3.837(1)$ Å, *Pnnm* space group (corresponding to a 125.6 $Å^3$ cell volume) [12]. In this marcasite structure (m-$NiSb_2$) the Ni atoms are octahedrally coordinated by six antimony atoms, with the calculated Ni–Sb average distance of 2.554 Å. $NiSb_6$ octahedra are arranged sharing two edges with adjacent octahedra parallel to *c*-axis (see Fig. 2). Two Ni atoms per unit cell occupy the crystallographic positions (2a) Ni (0 0 0) and four Sb atoms the positions (4g) Sb (0.219(1), 0.3593(8), 0). Each nickel atom is in $3d^6$ low-spin state. This compound has a predominantly covalent type of bonding. Like the antimonide compounds with the marcasite structure ($CrSb_2$, $FeSb_2$, $CoSb_2$), $NiSb_2$ has semiconductor behavior.

The powder morphology was investigated by scanning electron microscopy (right inset Fig. 1) showing 5–10 μm crystallites intimately nested to form 20–50 μm agglomerates.

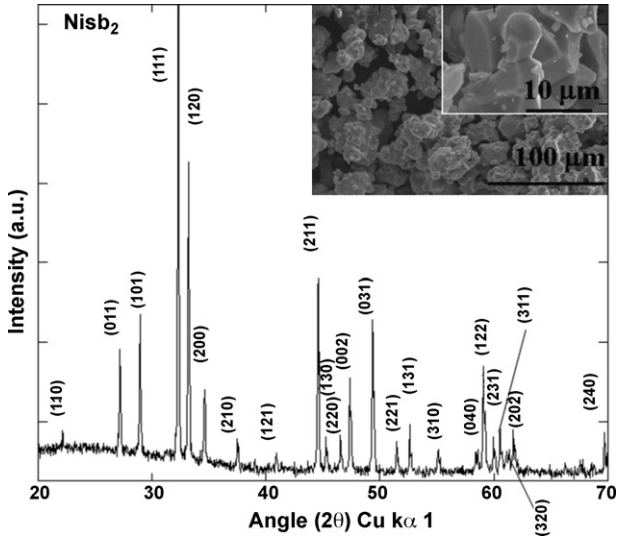

Fig. 1. X-ray diffraction patterns (Cu Kα) of the orthorhombic $NiSb_2$ phase prepared by a high temperature ceramic route. Inset shows the SEM image.

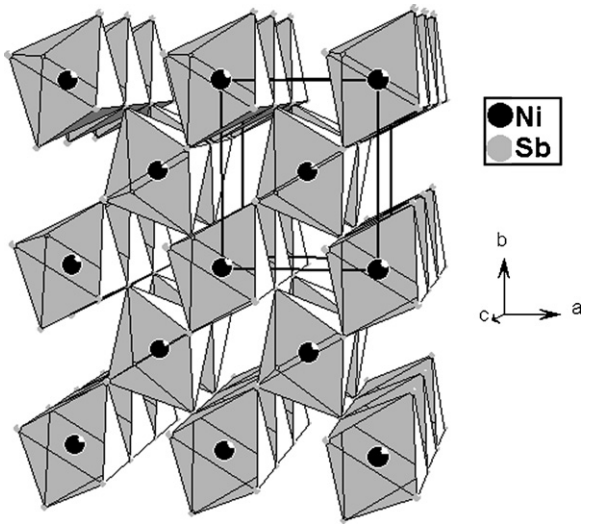

Fig. 2. The m-$NiSb_2$ orthorhombic structure ($a = 5.180(2)$ Å, $b = 6.312(2)$ Å, $c = 3.837(1)$ Å, *Pnnm* space group).

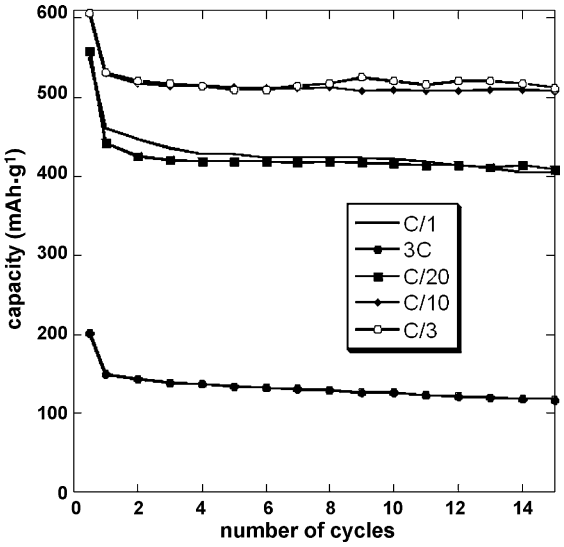

Fig. 4. The capacity retention of a $NiSb_2$/Li cell cycled at a *C*/*n* with $n = 0.33$, 1, 3, 10, 20 for the 15 first cycles.

3.2. Electrochemical properties

The $NiSb_2$/Li half-cell was assembled and tested using *C*/*n* rates ($n = 0.33$, 1, 3, 10, 20). Surprisingly the best electrochemical performances (plotted in Fig. 3) were obtained for a *C*/3 (1 Li/3 h) rapid cycling rate. A 15% capacity lost is observed (or 12% if we take into account the irreversible insertion in C_{black}) between the first discharge and the first charge. After this first cycle, there is no fading observed, which makes it possible to maintain a 520 mAh g^{-1} reversible capacity after 15 cycles (Figs. 3 and 4). At a rapid *C* rate, the reversible capacity obtained after 20 cycles reaches 410 mAh g^{-1} without any loss (Fig. 4). For a higher 3*C* rate, the capacity is drastically decreased to 120 mAh g^{-1}, while the cycling retention remains unmodified (Fig. 4).

During the first discharge down to 0 V, at *C*/3 rate, the voltage versus composition curve (Fig. 3) shows a total reaction of 6.85 Li^+ per $NiSb_2$ formula unit, correlated with a 600 mAh g^{-1} gravimetric capacity. During the initial 0.5 Li^+ uptake, a progressive decrease in the voltage down to 0.53 V was observed. This first process is partly associated with the insertion into the acetylene black. From 0.53 to 0.48 V a second step, characterized by an incremental peak at 0.52 V in the derivative curve plotted in Fig. 5, occurs. From 0.48 to 0.2 V a well-pronounced galvanostatic voltage plateau can be observed for the reaction of 4.0 Li^+ (Fig. 3). This process is characterized by the huge incremental peak centred at 0.43 V (Fig. 5) ascribable to a biphasic process. At the end of discharge, the galvanostatic curve shows a rapid potential decrease down to 0 V. Upon the succeeding charge, 5.85 Li^+ are extracted from the electrode,

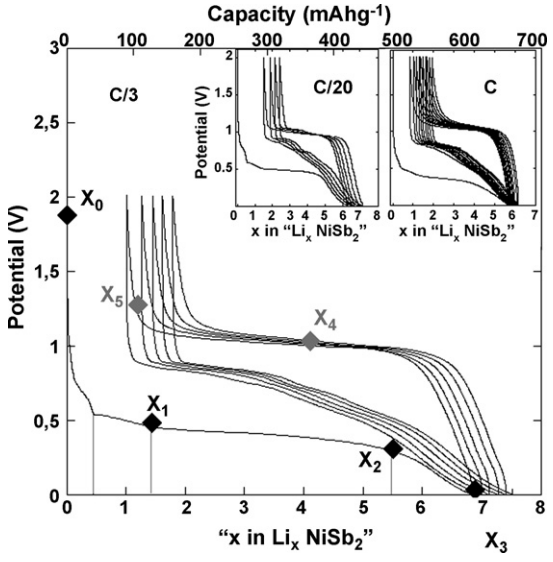

Fig. 3. The voltage-composition traces for a $NiSb_2$/Li cell between 2 and 0 V cycled at a *C*/3 rate and at a *C* and *C*/20 rate in right and left insets, respectively.

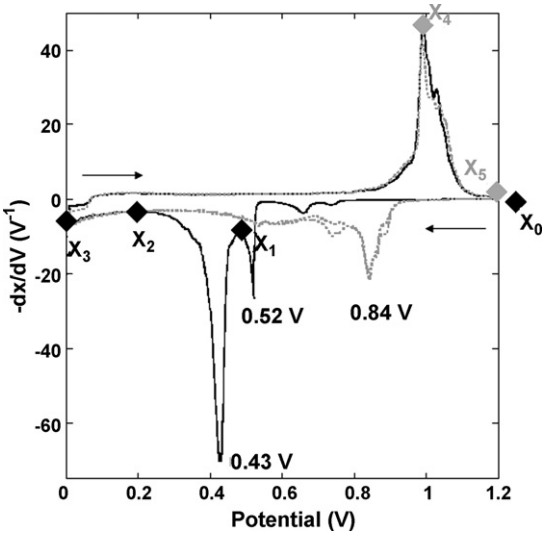

Fig. 5. The derivatives $-dx/dV$ plots are shown for the three first cycles for $NiSb_2$/Li cell (first cycle in black line, second and third cycle in grey line) cycled at a *C*/10 rate between 2 and 0 V.

corresponding to a reversible specific capacity of 500 mAh g^{-1} and a volumetric capacity of 4100 mAh cm^{-3}. A huge asymmetric incremental oxidative peak centred at 0.99 V, with a shoulder at 1.03 V, appears. Upon the second and further discharges, more complex processes occur from 0.94 to 0.4 V, while the charge profil appears to be unchanged. The $NiSb_2$/Li cell shows a very reproducible voltage profile upon subsequent cycles. It is worth noticing that the polarisation between the oxidation and reduction curve is reduced when the cycling rate decreases, which deals to clearly better define incremental peaks. To get deeper insights into these processes, both *ex situ* XRD and Mössbauer spectroscopy measurements at selected potential points were performed.

3.3. Ex situ X-ray diffraction

3.3.1. The first discharge

In Fig. 6, the X-ray powder pattern collected from the $NiSb_2$/Li cell discharged at 0.47 V (X_1, in Figs. 3 and 5, $x = 1.3$ Li) points out that the main Bragg peaks of the pristine $NiSb_2$ structure slightly shifted down to lower angles (inset, Fig. 6) and present a slight increase of the full width at half maximum (FWHM). At this stage of the electrochemical reaction, the refined parameters of the orthorhombic $NiSb_2$ structure in the *Pnnm* space group are: $a = 5.1908(4)$ Å, $b = 6.3284(4)$ Å, $c = 3.846(2)$ Å corresponding to a 126.3 $Å^3$ cell volume. This first process should correspond to a lithium insertion correlated with a small volume expansion (<1%). The second X-ray powder pattern, recorded at 0.2 V (X_2 point) after 5.5 reacted Li atoms, shows mainly a new set of broad diffraction peaks illustrated by stars in Fig. 6, centred at $2\theta = 23.7°$, 27.3°, 39.1° and 45.9°. These peaks can be attributed to the main Bragg peaks of the cubic-Li_3Sb polymorph ($a = 6.572$ Å, *Fm3m*) indexed with (1 1 1), (2 0 0), (2 2 0) and (3 1 1), respectively [13]. Note that the fcc Li_3Sb phase is designated in the Li/Sb phase diagram as the high temperature polyform (the ambient temperature αLi$_3$Sb transforms to β-Li_3Sb at a temperature above 650 °C).

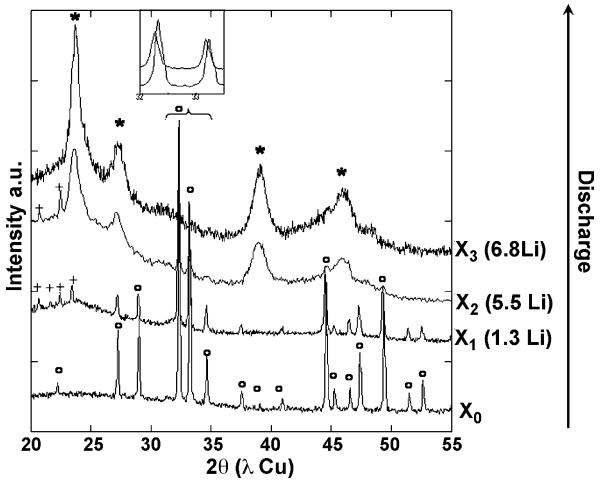

Fig. 6. *Ex situ* X-ray diffraction patterns collected during the discharge of a $NiSb_2$/Li electrochemical cell down to 0 V at a *C*/3 cycling rate. The Bragg peaks corresponding to m-$NiSb_2$ phase, to the Li_3Sb phase and to the X-ray holder are referred by empty cycles, stars and crosses, respectively.

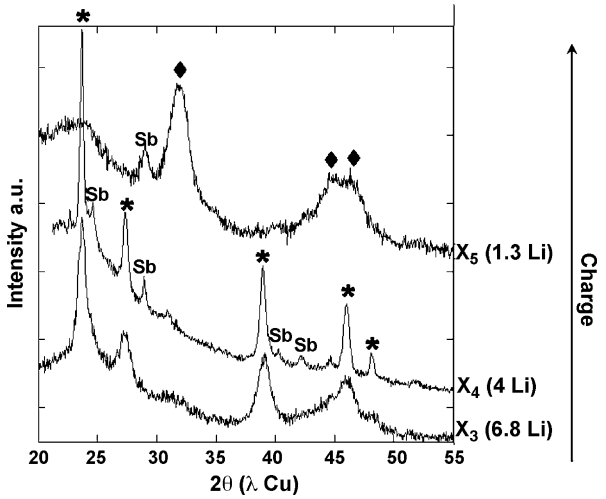

Fig. 7. *Ex situ* X-ray diffraction patterns collected during the charge of a $NiSb_2$/Li electrochemical cell up to 2 V at a *C*/3 cycling rate. The Bragg peaks related to the Li_3Sb phase, to the Sb phase and to the HP-$NiSb_2$ are referred by stars, Sb and diamonds, respectively.

The main Bragg peaks of the orthorhombic pristine $NiSb_2$ still appear at $2\theta = 32.2°$ and 33.2°. When the $NiSb_2$/Li cell is fully discharged at 0 V (X_3 point, $x = 6.8$ Li), only the cubic Li_3Sb main Bragg peaks remain. On the other hand, we could not point out any signs of peaks corresponding to the growth of metallic Ni, owing to their nanosized dimensions (well below the limit of detection by XRD).

3.3.2. The first charge

The powder patterns of the charged samples are plotted in Fig. 7. Surprisingly the powder collected from the $NiSb_2$/Li charged cell at 0.99 V (X_4 point, $x = 4$ Li) seems to be better crystallized than the electrode obtained at the end of discharge. This powder pattern is characterized by the presence of diffraction peaks characteristic of the Li_3Sb cubic phase and Sb rhomboedral phase ($a = 4.3$ Å, $c = 11.26$ Å, *R*-3*m*). At 1.2 V corresponding to the end of the oxidation process (X_5 point, $x = 1.3$ Li), the electrode is drastically modified, since a new set of broad and diffuse peaks is collected. These peaks cannot be attributed to the pristine $NiSb_2$ phase, while they perfectly correspond to the main Bragg peaks of the high-pressure $NiSb_2$ polymorph (*Pbca*, $a = 6.287(1)$ Å, $b = 6.364(1)$ Å, $c = 12.367(1)$ Å) recently described in the literature by Takizawa et al. [14]. The authors obtained this phase by high pressure/temperature treatment of normal marcasite-type $NiSb_2$ (m-$NiSb_2$ hereafter) at 6 GPa and 600 °C. The phase transition from the normal marcasite-type to the new polymorph is reversible and reproducible, indicating that this phase is a high-pressure polymorph of $NiSb_2$ (HP-$NiSb_2$ hereafter) [15]. In this new structure the Ni atom is octahedrally coordinated by six Sb atoms at six different bond distances in the range 2.53–2.6 Å. In the more symmetric m-$NiSb_2$ structure, only two Ni–Sb bonds exist (4× 2.438 Å and 2× 2.538 Å). The single crystallographic Sb site (8c) in the m-$NiSb_2$ is splitted in Sb1 and Sb2 (8c) sites in the HP-form (Fig. 8). In the HP-form, the distortion of the $NiSb_6$ octahedron is how-

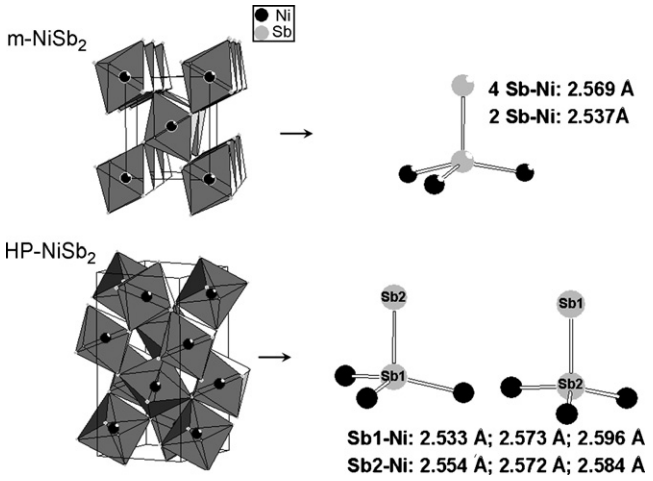

Fig. 8. Local environments of nickel and antimony atoms in m-$NiSb_2$ (top) and HP-$NiSb_2$ (bottom) phases.

ever somewhat larger involving Ni–Sb–Sb angle modifications. The main difference between HP- and m-$NiSb_2$ is found in the linkage of $NiSb_6$ octahedra (Fig. 8), presumably caused by a change in the ligand field. In the m-$NiSb_2$, $NiSb_6$ octahedra are arranged by sharing two edges with adjacent octahedra parallel to *c*-axis (Fig. 2). In contrast $NiSb_6$ octahedra are linked to adjacent octahedral by sharing one edge and four corners in HP-$NiSb_2$. This leads to effective packing of $NiSb_6$ octahedra accompanied with a 2% volume decrease, as compared to the ambient pressure form. The HP-$NiSb_2$ can be viewed as an intermediate structure between the marcasite-type structure and the more packing pyrite structure, in which the $NiSb_6$ octahedra are connected with adjacent octahedra by sharing their corners [14].

3.4. Mössbauer study

A Mössbauer study was undertaken in order to confirm the presence of Li_3Sb in the discharged electrode and to identify the antimonide intermediate phases in the charged electrode (Table 1).

Fig. 9, M0 shows the ^{121}Sb Mössbauer spectrum recorded for the starting electrode. It reveals the presence of two phases. A singlet (with hyperfine parameters $\delta = -1.65\ mm\ s^{-1}$, $eQV_{zz} = 6.37\ mm\ s^{-1}$ and 94% relative contribution) is characteristic of the m-$NiSb_2$ phase, in good agreement with the description given in the literature [16]. The second singlet was attributed to the presence of the phase Sb_2O_5 as impurity not detected by X-ray diffraction ($\delta = 8.89\ mm\ s^{-1}$ and $eQV_{zz} = -3.70\ mm\ s^{-1}$ and 6% relative contribution) [17]. Note that this oxide is systematically detected as a side product in the different cycled samples. The spectrum obtained at 0.47 V (M1 sample) shows three components: 84% of $NiSb_2$, Sb_2O_5 and a new small contribution ascribable to Li_3Sb ($\delta = 1.17\ mm\ s^{-1}$ and 4% relative contribution) [18]. In the following discharged samples (M2 and M3) the Li_3Sb relative contribution increases, while the $NiSb_2$ pristine material contribution decreases. At the end of discharge (M4 point) the relative contribution of Li_3Sb is greater than 82%, and a small contribution of unreacted $NiSb_2$ still appears (6% relative contribution).

These results confirm the following reductive reaction based on the simple equation:

$$m\text{-}NiSb_2 + 6Li \rightarrow 2Li_3Sb + Ni \quad (2)$$

Table 1
^{121}Sb Mössbauer parameters obtained from spectra recorded for the M0 to M6 compositions (Fig. 9)

Sample	*U* (V), *x* Li	δ (mm s^{-1})	eQV_{zz} (mm s^{-1})	Γ (mm s^{-1})	*C* (%)	Identification
M0	2.84 V, 0	−1.65 (2)	6.37 (9)	1.79 (6)	94 (3)	$NiSb_2$
		8.89 (0)	−3.70 (1)	1.79 (6)	6 (3)	Sb_2O_5
M1	0.47 V, 1.3	−1.54 (2)	6.35 (2)	1.60 (5)	84 (2)	$NiSb_2$
		1.17 (1)	–	1.60 (5)	4 (2)	Li_3Sb
		8.85(0)	−3.60 (1)	1.60 (5)	12 (2)	Sb_2O_5
M2	0.35 V, 3.8	−1.53 (3)	6.44 (4)	1.75 (4)	53 (2)	$NiSb_2$
		1.15 (5)	–	1.75 (4)	36 (3)	Li_3Sb
		8.84 (0)	−3.60 (1)	1.75 (4)	11 (2)	Sb_2O_5
M3	0.2 V, 5.5	−1.6 (2)	6.46 (2)	1.69 (7)	30 (1)	$NiSb_2$
		1.05 (1)	–	1.69 (7)	58 (1)	Li_3Sb
		8.84 (1)	−3.60 (1)	1.69 (7)	12 (2)	Sb_2O_5
M4	0.0 V, 6.8	−1.65 (4)	6.40 (1)	1.79 (4)	6(5)	$NiSb_2$
		1.02 (4)	–	1.79 (4)	82 (5)	Li_3Sb
		8.89 (3)	−3.70 (2)	1.79 (4)	12 (1)	Sb_2O_5
M5	0.99 V, 4	−1.06 (6)	7.22 (1)	1.70 (2)	41 (5)	$NiSb_2$-HP
		−3.25 (2)	3.20 (3)	1.70 (2)	7 (2)	Sb
		1.02 (4)	–	1.70 (2)	46 (3)	Li_3Sb
		9.09 (3)	−3.70 (0)	1.70 (2)	6 (3)	Sb_2O_5
M6	1.2 V, 1.3	−1.06 (3)	7.59 (3)	1.67 (3)	62 (3)	$NiSb_2$-HP
		−3.29 (2)	3.20 (2)	1.67 (3)	32 (3)	Sb
		8.97 (1)	−3.72 (0)	1.67 (3)	6 (3)	Sb_2O_5

δ: isomer shift relative to InSb (−8.72 mm s^{-1} relatively to $Ba^{121m}SnO_3$ source), eQV_{zz}: quadrupole splitting, Γ: linewidth, *C*: relative contribution.

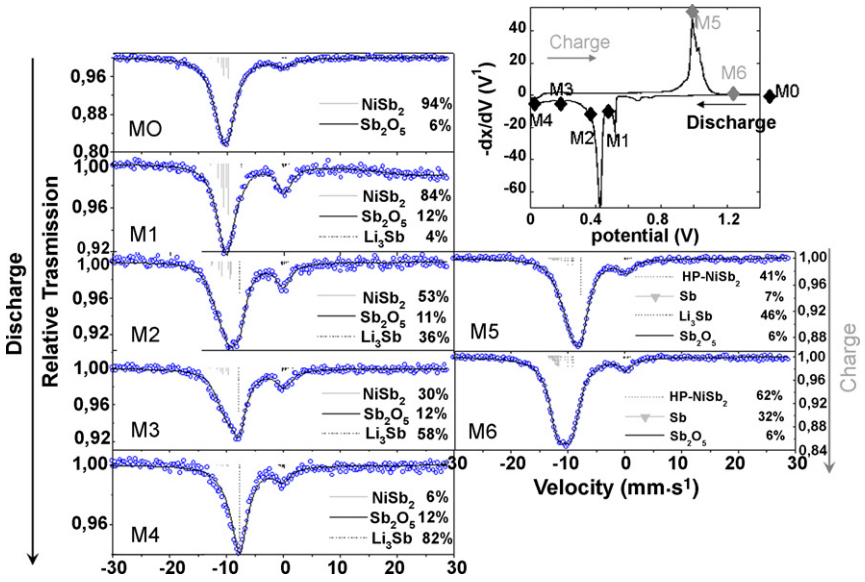

Fig. 9. ^{121}Sb Mössbauer spectra from $NiSb_2$/Li sample at a *C*/3 rate for the pristine electrode (M0), for the partially discharged electrode at 0.47 V (M1), at 0.35 V (M2) and at 0.2 V (M3), for the fully discharged electrode at 0 V (M4) and for the partially charged electrode at 0.99 V (M5) and at 1.2 V (M6).

On charge, at 0.99 V (M5 sample), Li_3Sb contributes to 46% of the total spectrum, while two new signals appear at $\delta = -3.25\,mm\,s^{-1}$ and $eQV_{zz} = 3.20\,mm\,s^{-1}$ and at $\delta = -1.06\,mm\,s^{-1}$ and $eQV_{zz} = 7.22\,mm\,s^{-1}$, respectively. The former is clearly assigned to Sb [19], while it is more complex to identify the latter. It cannot be assigned to m-$NiSb_2$ whose signal is expected to appear at $\delta = -1.65\,mm\,s^{-1}$. For the M6 sample, corresponding to the end of charge (1.2 V), the signal with the $-1.06\,mm\,s^{-1}$ isomeric shift ($eQV_{zz} = 7.59\,mm\,s^{-1}$) has the majority ratio (62% relative contribution) and the antimony signal a 32% relative contribution.

By combining the *ex situ* XRD results and the Mössbauer analysis a global oxidative reaction based on Eq. (3) can be proposed:

$$5/3\,Li_3Sb + 2/3\,Ni - 5Li \rightarrow 2/3\,HP\text{-}NiSb_2 + 1/3\,Sb \qquad (3)$$

Note that the Mössbauer signal of the high-pressure $NiSb_2$ form is unknown in the literature. However the HP-$NiSb_2$ crystallographic structure is well depicted as previously mentioned in this paper [14]. The HP-$NiSb_2$ shows an intermediate structure between the marcasite-type and the more packing pyrite structures. ^{121}Sb Mössbauer studies on compounds with pyrite and marcasite-type structures was published in the past and showed that there is a correlation between the quadrupole splitting and the average angular distortion from tetrahedral symmetry around the Sb sites [16]. As shown in the first part, the HP-$NiSb_2$ structure presents a notable angular distortion from tetrahedral symmetry around the Sb sites. The $eQV_{zz} = 7.59\,mm\,s^{-1}$ measured upon charge at the M6 point is greater than the quadrupole splitting at the M0 point (characteristic of the m-$NiSb_2$) $eQV_{zz} = 6.37\,mm\,s^{-1}$. This trend has to be correlated to the increase of the average angular distortion from tetrahedral symmetry around the Sb sites, from the m-$NiSb_2$ to the more distorded HP-$NiSb_2$.

4. Discussion

Firstly, the electrochemical results of the m-$NiSb_2$/Li half-cell are indicative of a highly reversible conversion reaction. On discharge, after a first insertion process of less than 1 Li^+ in m-$NiSb_2$, associated with a limited volume expansion (<1%), a biphasic reaction takes place, converting the Li_xNiSb_2 phase ($x < 1$) to the (fcc-Li_3Sb + Ni^0) composite electrode. The formation of the high temperature-Li_3Sb phase instead of the hexagonal low temperature-Li_3Sb phase emphasizes the complexity of the thermodynamical properties in the conversion processes. The further discharge also leads to the Li_3Sb matrix and the Ni particles.

It is interesting to note that the m-$NiSb_2$ and the NiP_2 phases behave similarly with a conversion to Li_3Pn (Pn = P, Sb) and Ni^0 nanoparticles during the first discharge. However, upon charge, the electrochemical mechanism appears to be different for both pnictides. For the di-antimonide, the lithium extraction from the discharged electrode leads to the formation of high pressure HP-$NiSb_2$ and Sb phases. This process induces that a part of Ni^0 particles of the discharged electrode does not react upon charge.

For the phosphide no trace of HP-NiP_2 (cubic NiP_2 polyform) was identified upon charge [9]. So far, for the reactions of intermetallic phases versus lithium, a reversible process leading to a more packing polymorph phase at the end of charge has never been observed. Chemical bond analysis and Li–Ni–Sb phase diagram based on first principles DFT computations should be helpful to understand this transformation.

As for the conversion reactions so far reported with oxides, sulphides or fluorides (excepted of phosphides), the measured amount of Li uptake (6.85 Li^+) during the first discharge in $NiSb_2$ is greater than the theoretical one (6 Li^+). The extra capacity is usually associated either to a reversible growth of an electrochemically gel-like polymer layer or to a reversible heterogeneous interfacial storage mechanism.

Another universal characteristic of the conversion reactions is the existence of a large potential difference between the first and second discharge, a few hundreds of mV, usually viewed as a kinetic limitation [8,9] corresponding to the necessary potential to provide the required activation energy to trigger the conversion reaction. Once this formation step achieved, due to the nano character of the formed composite, the second discharge is kinetically less limited and occurs at higher voltage. For $NiSb_2$, the potential difference between the first discharge and charge increases from 0.2–0.4 V for the slower rate (*C*/20) to 0.4–0.8 V for the more rapid cycling rate (*C*). However the higher capacity as well as the best capacity retention were obtained for the rapid cycling rate. For this compound, the cycling rate does not appear to be a kinetic limitation since the performances are improved with increasing the cycling rate.

5. Conclusions

The advantage of $NiSb_2$, compared with other antimonides, does not lie on its large reversible capacity but rather on its ability to sustain (after the first discharge) 100% of its capacity over 15 cycles as well as on its aptitude to deliver its full capacity at rapid rate. That performance originates in an original reversible process converting m-$NiSb_2$ to ($Li_3Sb + Ni^0$) upon the first discharge, and transforming this composite electrode into the high-pressure $NiSb_2$ form upon charge. The stabilization of this high pressure phase at ambient temperature and pressure shows the difficulties to evaluate the thermodynamical parameters in the battery, especially for conversion materials. Different synthetic routes are currently in progress to synthesize the HP-$NiSb_2$ form. The comparison between the as-prepared HP-$NiSb_2$/Li cell discharge and the second discharge of the m-$NiSb_2$/Li cell, will definitively confirm the mechanism.

Moreover electronic band calculations will tell us why the more packing HP-$NiSb_2$ structure is stabilized on charge rather than the marcasite ambient pressure form. A coupled Mössbauer/XRD study is also in progress to identify the intermediate phases formed during the second and further discharges.

Acknowledgment

Authors are grateful to Nicolas Gagne for helpful discussions.

References

[1] R. Alcantara, F.J. Fernandez-Madrigal, P. Lavela, J.L. Tirado, J.-C. Jumas, J. Olivier-Fourcade, J. Mater. Chem. 9 (1999) 2517.
[2] J.-M. Tarascon, M. Morcrette, L. Dupont, Y. Chabre, C. Payen, D. Larcher, V. Pralong, J. Electrochem. Soc. 150 (2003) A732.
[3] I. Devos, M. Womes, M. Heilemann, J. Olivier-Fourcade, J.-C. Jumas, J.L. Tirado, J. Mater. Chem. 14 (2004) 1759.
[4] C.M. Ionica, L. Aldon, P.E. Lippens, F. Morato, J. Olivier-Fourcade, J.-C. Jumas, Hyperfine Interact. 156/157 (2004) 555.
[5] J. Xie, X.B. Zhao, G.S. Cao, M.J. Zhao, Y.D. Zhong, L.Z. Deng, Mater. Lett. 57 (2003) 4673.
[6] F.J. Fernandez-Madrigal, P. Lavela, C. Perez-Vicente, J.L. Tirado, J. Electroanal. Chem. 501 (2001) 205.
[7] L.M.L. Fransson, J.T. Vaughey, R. Benedek, K. Edström, J.O. Thomas, M.M. Thackeray, Electrochem. Commun. 3 (2001) 317.
[8] P. Poizot, S. Laruelle, S. Grugeon, L. Dupont, J.-M. Tarascon, Nature 407 (2000) 496.
[9] F. Gillot, S. Boyanov, L. Dupont, M.-L. Doublet, M. Morcrette, L. Monconduit, J.-M. Tarascon, Chem. Mater. 17 (2005) 6327.
[10] C.M. Ionica, P.E. Lippens, J. Olivier-Fourcade, J.-C. Jumas, J. Power Sources 146 (2005) 478.
[11] J. Xie, X.B. Zhao, G.S. Cao, M.J. Zhao, S.F. Su, J. Alloys Compd. 393 (2005) 283.
[12] A. Kjekshus, T. Rakke, A.F. Andresen, Acta Chem. Scand. 28 (1974) 996.
[13] Brauer Zintl, Z. Phys. Chem. (Leipzig) 37 (1937) 323.
[14] H. Takizawa, K. Uheda, T. Endo, Intermetallics 8 (2000) 1399.
[15] M.E. Fleet, Am. Mineral. 57 (1972) 1.
[16] J.D. Donalson, A. Kjekshus, D.G. Nicholson, M.J. Tricker, Acta Chem. Scand. 26 (1972) 3215.
[17] L. Bowen, J. Inorg. Nucl. 33 (1971) 953.
[18] L. Aldon, A. Garcia, J. Olivier-Fourcade, J.-C. Jumas, F.J. Fernandez-Madrigal, P. Lavela, C. Perez Vicente, J.-L. Tirado, J. Power Sources 119 (2003) 585.
[19] P.E. Lippens, Solid State Commun. 113 (2000) 399.